EPJ manuscript No.
(will be inserted by the editor)

Systematics of collective correlation energies from self-consistent mean-field calculations

P. Klüpfel[1], J. Erler[1], P.–G. Reinhard[1], and J. A. Maruhn[2]

[1] Institut für Theoretische Physik, Universität Erlangen, Staudtstrasse 7, D-91058 Erlangen, Germany
[2] Institut für Theoretische Physik, Universität Frankfurt, Max-von-Laue-Str. 1, D-60438 Frankfurt a. M., Germany

November 10, 2008/ Received: date / Revised version: date

Abstract. The collective ground-state correlations stemming from low-lying quadrupole excitations are computed microscopically. To that end, the self-consistent mean-field model is employed on the basis of the Skyrme-Hartre-Fock (SHF) functional augmented by BCS pairing. The microscopic-macroscopic mapping is achieved by quadrupole-constrained mean-field calculations which are processed further in the generator-coordinate method (GCM) at the level of the Gaussian overlap approximation (GOA). We study the correlation effects on energy, charge radii, and surface thickness for a great variety of semi-magic nuclei. A key issue is to work out the influence of variations of the SHF functional. We find that collective ground-state correlations (GSC) are robust under change of nuclear bulk properties (e.g., effective mass, symmetry energy) or of spin-orbit coupling. Some dependence on the pairing strength is observed. This, however, does not change the general conclusion that collective GSC obey a general pattern and that their magnitudes are rather independent of the actual SHF parameters.

PACS. 2 1.10.Dr, 21.10.Ft, 21.10.Re, 21.60.Ev, 21.60.Jz

1 Introduction

The nucleus is a highly correlated many-body system and thus the topic of correlations has always accompanied nuclear physics. Short-range correlations dominate due to the huge short-range repulsion in the nucleon-nucleon interaction. Their treatment requires very involved approaches as, e.g., Brueckner-Hartree-Fock, variational Jastrow, hyper-netted chain, or no-core shell model calculations, see e.g. [1,2,3,4,5]. Large-scale applications employ simpler approaches, among which the most microscopic ones are self-consistent mean-field models based on effective energy-density functionals or effective forces, respectively. The functional is motivated by a formal derivation from an underlying many-body approach, see e.g. [6], but adjusted phenomenologically because of the as yet insufficient input from ab-initio models; for a recent review see [7]. A widely used functional is, e.g., the Skyrme-Hartree-Fock (SHF) approach. However obtained, the nuclear energy-density functional is supposed to contain all crucial correlations effectively. The reasoning is quite similar to that of density-functional theory in electronic systems where theorems and clean theoretical developments have come much farther, for an overview see [8]. The perfect functional thus allows describing a system by a mere mean-field calculation and yet obtaining the correct energy and density. That ideal functional is known to be highly non-analytic to account for the sudden changes from one particle number to another [8]. Actual functionals, however, are rather smooth functions of the involved densities, partially owing to approximations in their derivation and partially for practical reasons of manageability. This, in turn, means that the functional can incorporate only the smooth trends of the correlations and will probably fail to account for quickly changing contributions. Yet such effects are known to exist in the nuclear landscape. The nuclear shell structure leads to dramatic changes in the nuclear shape when adding or removing nucleons, known as the nuclear Jahn-Teller effect [9,10]. Pairing moderates these strong fluctuations [9,11], but sizeable fluctuations remain as can be seen from the changes in the low-energy spectra along isotopic or isotonic chains [12]. The lowest excitation in even-even nuclei is in most cases a quadrupole state assigned as 2_1^+. This 2_1^+ state is a collective state. It is associated with substantial recoupling of the simple mean-field excitations which, in turn, produces significant correlation effects. These collective correlations are not smooth with changing particle number and thus are not included in the energy-density functional. They have to be added explicitly. That has been discussed for decades, but mostly based on semi-empirical estimates, see e.g. [13, 14]. Thorough calculations based on self-consistent mean-field models have also been tried for a long time; see e.g. [15,16,17,18]. Extensive surveys running over all nuclear landscapes based on SHF have been published recently [19,20,21] and there exists also a systematic study using the Gogny force [22] showing very similar trends. It is the aim of this paper to give a survey of collective correla-

tions within the SHF mean field, exploring in detail the dependence on the SHF functional. The aim is to prepare ground for a revision of the phenomenological adjustment of SHF by finding out the least correlated nuclei.

The low-lying quadrupole states can be formulated in terms of the Bohr-Hamiltonian, which establishes collective dynamics in the five quadrupole degrees of freedom [23]. The parameters of the collective Hamiltonian are usually adjusted phenomenologically, see e.g. the applications in [24] and more recently in the interacting boson model [25]. The direct connection between a microscopic description and a collective picture can be established by a collective path, which consists of a continuous series of mean-field states with prescribed deformations, produced by a quadrupole constraint. The mapping of the path into collective dynamics is established by virtue of the generator coordinate method (GCM). [26,27]. The complex integral equations of the GCM can be simplified using the Gaussian-Overlap-Approximation (GOA) which, furthermore, allows to establish contact between the microscopic foundation and the collective Bohr-Hamiltonian [28,17]. In practice, there are, on the one hand, fully fledged GCM calculations which skip the collective Hamiltonian as intermediate level and compute low-energy spectra directly from the coherent superposition of the collective path; these sophisticated calculations imply exact projection for the conserved quantities, like particle number, angular momentum, and center of mass; from the many published results we mention here [29,30] as two recent examples. On the other hand, there are the techniques which use the Bohr-Hamiltonian as an intermediate stage, for an early example see [15,16] and for more recent achievements [31, 32]. We are going here to use the GCM-GOA. The path is generated from axially deformed SHF-BCS states. The full five-dimensional topology is regenerated by interpolation into the triaxial plane in an extension of the method presented in [33]. The interpolation scheme promises reliable results for vibrators whose collective deformation rarely reaches large values. It is thus well suited for the present survey dealing with chains of semi-magic nuclei.

2 Formal framework

2.1 The Skyrme mean-field model

The starting point for the self-consistent microscopic description is the SHF energy functional $E = E(\rho, \tau, \mathcal{J}, \mathbf{j}, \sigma)$, which is expressed in terms of a few local densities and currents obtained as sums over single-particle wave functions: density ρ, kinetic density τ, spin-orbit density $\mathcal{J}$, current $\mathbf{j}$, and spin density σ, each occurring twice, once for protons and once for neutrons. It is augmented by a pairing functional deduced from a zero-range two-body force (DI=delta interaction) or combined with a density dependence (DDDI=density-dependent delta interaction) [34]. They are described with the pairing functional

$$E_{\rm pair} = -\sum_{q\in p,n} \frac{V_{0q}}{4} \int d^3\mathbf{r} \left[1 - \frac{\rho(\mathbf{r})}{\rho_0}\right] \Re\{\chi_q(\mathbf{r})\}^2 \qquad (1)$$

where DDDI-pairing corresponds to $\rho_0 = 0.159\,\mathrm{fm}^{-3}$, while DI-pairing is recovered for $\rho_0 \to \infty$. The pair density is $\chi(\mathbf{r}) = \sum_\alpha u_\alpha v_\alpha |\varphi_\alpha(\mathbf{r})|^2$. The real part thereof confines the contributions to time-even parts. This coincides with the standard pairing functional for stationary states (where χ is purely real) and it implies that time-odd pairing effects in dynamical response are ignored. Pairing is treated within the BCS approximation and augmented by the Lipkin-Nogami (LN) correction which serves to force a minimal amount of pairing everywhere and so prevents the sudden changes associated with the pairing phase transition. That smoothing is compulsory for the further processing of the mean-field states in the description of collective dynamics. The BCS approximation is applicable for well bound nuclei where the Fermi energies are safely below the continuum threshold. This holds for the nuclei considered here along the whole collective deformation path. For details about SHF, BCS and LN, see the review article [7].

The mean-field equations are derived variationally from the given energy functional. They determine the ground state or a locally stable isomer. Collective motion goes through a succession of deformed mean fields, the collective path. The low-lying quadrupole mode is particularly soft and the collective path is related to quadrupole deformed shapes. We generate the path by imprinting a dedicated deformation using quadrupole-constrained mean-field equations, often called constrained Hartree-Fock (CHF),

$$\hat{H}_{\rm MF}|\Phi_{\alpha_{20}}\rangle = \mathcal{E}|\Phi_{\alpha_{20}}\rangle \quad , \qquad (2a)$$

$$\hat{H}_{\rm MF} = \hat{h}_{\rm MF} - \epsilon_{\rm F}\hat{N} - \lambda\hat{Q}_{20} \quad , \qquad (2b)$$

where $\hat{h}_{\rm MF}$ is the SHF-BCS mean field Hamiltonian (depending on the local densities and thus on the state $|\Phi_{\alpha_{20}}\rangle$), $\epsilon_{\rm F}$ is the Fermi energy, and λ the Lagrange parameter for the quadrupole constraint. $\hat{Q}_{20}$ is the quadrupole operator and α_{2m} its dimensionless expectation value, i.e.

$$\hat{Q}_{2m} = r^2 Y_{2m} f_{\rm cut}(\mathbf{r}) \quad , \qquad (2c)$$

$$\alpha_{2m} = \frac{4\pi}{5} \frac{\langle\Phi_{\alpha_{20}}|r^2 Y_{2m}|\Phi_{\alpha_{20}}\rangle}{Ar^2} \quad , \qquad (2d)$$

with A the total particle number and r the r.m.s. radius. The index m can run over $-2, -1, 0, 1$ and 2. For a while, we will consider only $m = 0$ which corresponds to axially symmetric deformations. The states are labeled with the dimensionless quadrupole moment (2d). The quadrupole operator is modified by a Wood-Saxon-like damping function $f_{\rm cut}$ with an extension of three times the nuclear radius and width of 1 fm in order to suppress the unbound regions from the asymptotics $\propto -x^2, -y^2$, or $-z^2$ [35]. The equations are solved with an extra iterative loop to maintain a wanted value of α_{20} [36]. This is done for a dense set of deformations α_{20}. At the end we have the collective path $\{|\Phi_{\alpha_{20}}\rangle\}$ as a series of mean-field states along which the collective motion can evolve. Its further processing will be discussed in section 2.2. Before carrying on, we ought to mention that the optimal scheme for generating a collective path is adiabatic time-dependent

Hartree-Fock (ATDHF) which generates the constraints in a self-consistent manner without imposing a preconceived idea of the collective deformation, see e.g. [28,37]. Experience shows that the quadrupole constraint is a good approximation in cases where the low lying 2_1^+ state is a truly collective mode. That applies practically to all nuclei, except for the doubly-magic ones. Thus our results near doubly-magic nuclei have to be taken with care.

The SHF functional sets only a framework within which there is a manifold of different parameterizations. Most available parameter sets describe ground states properties equally well but differ in other observables like, e.g., excitation spectra or nuclear matter properties [7]. One thus should consider several sufficiently different parameterizations to distinguish particular features of a given parameterization from general features of SHF. We will consider the following standard Skyrme parameterizations: SkM* as a widely used traditional standard [38], Sly6 as a recent fit which includes information on isotopic trends and neutron matter [39], and SkI3 as a recent fit which maps the relativistic iso-vector structure of the spin-orbit force [40]. The set contains distinct effective masses where SkM* has $m^*/m = 0.8$ while SLy6 and SkI3 have significantly lower values (0.69, or 0.6 respectively). SkI3 differs in that it has basically no proton-neutron coupling in the spin-orbit mean field. Thus all three forces differ somewhat in the actual shell structures they produce. Besides the effective mass, the bulk parameters (equilibrium energy and density, incompressibility, symmetry energy) are comparable. In addition, we employ a set with a systematic variation of effective mass, symmetry energy and spin-orbit force [41] to explore the sensitivity to these aspects of the force.

2.2 The collective Hamiltonian

Large-amplitude collective motion proceeds along the collective path, a series of mean-field states which differ very little in energy. Its description requires a coherent superposition of the states along the collective path. That is done in the framework of the GCM. The GOA allows to map the microscopic picture into a collective Hamiltonian for the five quadrupole degrees of freedom $\boldsymbol{\alpha} = (\alpha_{2-2}, \alpha_{2-1}, \alpha_{20}, \alpha_{21}, \alpha_{22})$ [28]. The final result is summarized briefly.

The collective Schrödinger equation to be solved reads

$$\left(\hat{H}^{\rm coll} - \delta\epsilon_{\rm F}\hat{N}^{\rm coll}\right)\phi(\boldsymbol{\alpha}) = E_n^{\rm coll}\phi(\boldsymbol{\alpha}) \quad , \tag{3}$$

with the collective Hamiltonian

$$\hat{H}^{\rm coll} = -\frac{1}{4}\left\{\nabla_\mu, \{B^{\mu\nu}(\boldsymbol{\alpha}), \nabla_\nu\}\right\} + V(\boldsymbol{\alpha}) \quad . \tag{4}$$

It is obtained from the general rules of a collective map which apply analogously to the collective map $\hat{N}^{\rm coll}$ of the particle-number operator [28]. The details are given here for the Hamiltonian. The potential in $\hat{H}^{\rm coll}$ is given by the mean-field energy from which the spurious contributions from rotational, vibrational, and center-of-mass zero-point energies are subtracted, i.e.

$$V(\boldsymbol{\alpha}) = E_{\rm SHF}(\boldsymbol{\alpha}) - E_{\rm ZPE}(\boldsymbol{\alpha}) - E_{\rm cm}(\boldsymbol{\alpha}) \quad , \tag{5a}$$

$$E_{\rm ZPE}(\boldsymbol{\alpha}) = \frac{1}{2}\lambda_{\mu\nu}B^{\mu\nu} - \frac{1}{4}(\lambda^{-1})^{\mu\nu}\nabla_\mu\nabla_\nu E_{\rm SHF} \quad , \tag{5b}$$

$$\lambda_{\mu\nu}(\boldsymbol{\alpha}) = \langle\Phi_{\boldsymbol{\alpha}}|\left\{\hat{\mathcal{P}}_\mu, \hat{\mathcal{P}}_\nu\right\}|\Phi_{\boldsymbol{\alpha}}\rangle \quad , \tag{5c}$$

$$\hat{\mathcal{P}}_\mu|\Phi_{\boldsymbol{\alpha}}\rangle = \mathrm{i}\frac{\partial}{\partial\alpha^\mu}|\Phi_{\boldsymbol{\alpha}}\rangle \ . \tag{5d}$$

where the $\hat{\mathcal{P}}_\mu$ are the generators of a change in the quadrupole momentum. The inverse collective mass tensor is evaluated as in terms of the constraint mean-field Hamiltonian $\hat{H}_{\rm MF}$ and the

$$B^{\mu\nu}(\boldsymbol{\alpha}) = \frac{1}{2}\langle\Phi_{\boldsymbol{\alpha}}|\left[\hat{\mathcal{Q}}^\mu, \left[\hat{H}_{\rm MF}, \hat{\mathcal{Q}}^\nu\right] - \mathrm{i}\hat{h}_{\mathrm{resp},\mathcal{Q}}\right]|\Phi_{\boldsymbol{\alpha}}\rangle \tag{6a}$$

where $\hat{\mathcal{Q}}^\mu$ are the generators of a dynamical boost. They are determined self-consistently as dynamical linear response to the collective momentum $\hat{\mathcal{P}}_\nu$, i.e.

$$\left(\mathrm{i}\left[\hat{H}_{\rm MF}, \hat{\mathcal{Q}}^\mu\right] + \hat{h}_{\mathrm{resp},\mathcal{Q}}\right)|\Phi_{\boldsymbol{\alpha}}\rangle = 2B^{\mu\nu}\hat{\mathcal{P}}_\nu|\Phi_{\boldsymbol{\alpha}}\rangle \quad , \tag{6b}$$

where $\hat{H}_{\rm MF}$ is the mean-field Hamiltonian belonging to state $|\Phi_{\boldsymbol{\alpha}}\rangle$ and $\hat{h}_{\mathrm{resp},\mathcal{Q}}$ is the response Hamiltonian for time-odd perturbations about $|\Phi_{\boldsymbol{\alpha}}\rangle$ [42]. The mass thus obtained is called self-consistent or ATDHF mass. It is to be noted that most straightforward GCM calculations omit the dynamical linear response and deal with an approximate mass which can be deduced purely from the static configurations. That amounts to replacing the dynamical boost operator $\hat{\mathcal{Q}}^\mu$ in formula (6a) simply by the redundant complement to $\hat{\mathcal{P}}^\mu$ [28], i.e.

$$\hat{\mathcal{Q}}^\mu|\Phi_{\boldsymbol{\alpha}}\rangle = -\mathrm{i}(\lambda^{-1})^{\mu\nu}\hat{\mathcal{P}}_\nu|\Phi_{\boldsymbol{\alpha}}\rangle \quad . \tag{7}$$

Accounting for the dynamical response explores the dynamic path for slow collective motion. Within the assumptions of the GOA framework it thus corresponds to a dynamic generator-coordinate method (DGCM). We will compare later on these two approaches to the collective mass. The collective path $|\Phi_{\boldsymbol{\alpha}}\rangle$ is computed for axially symmetric shapes, i.e. along α_{20}. This determines the raw collective potential $E_{\rm SHF}$, the masses B^{00} and the widths λ_{00} along the α_{20}. By a slight rotation of the nucleus, generated by the angular momentum operator $\hat{J}_x$ or $\hat{J}_y$, the moments of inertia are evaluated providing additional information about rotational properties of the nucleus. Including this information allows to evaluate the $B^{1,-1}$ and $\lambda_{1,-1}$ components of the GOA tensors. The data from prolate ($\alpha_{20} > 0$) and oblate ($\alpha_{20} < 0$) configurations are interpolated into the triaxial plane with methods similar to those employed in [33] but now accounting for the topology of the five dimensional quadrupole configuration space (see appendix A). The requirement of rotational symmetry for the collective Hamiltonian $\hat{H}^{\rm coll}$ and of smoothness in the triaxial direction allows to determine all needed ingredients of the collective Hamiltonian in the full triaxial

plane, for the regime of small deformations. It is to be noted that the assumption of small deformations limits the present treatment to nearly spherical nuclei. These are the ones which we will study in the following.

Coming back to the collective Schrödinger equation (3), we see that it contains a constraint on particle number. Each mean-field state $|\Phi_{\alpha_{20}}\rangle$ is tuned to the same average particle number $\langle\hat{N}\rangle = N$ by tuning the Fermi energy in the mean-field Hamiltonian (2b). But the coherent superposition may lead to a small drift of the average particle number. The term $\propto \delta\epsilon_{\rm F}$ in (3) serves for a final particle-number correction (PNC).

3 Results and discussion

3.1 Ground-state correlations of semi-magic nuclei

Figure 1 shows the results of the SHF plus DGCM-GOA calculations for the correlation effects on the four bulk observables energy E, charge r.m.s. radius r, diffraction radius R, and surface thickness σ for all semi-magic nuclei considered in this survey. The upper panel complements that by the energies of the low lying 2^+ compared with the experimental results (taken from [43]). That figure is generic in the sense that the trends seen here are typical for a great variety of Skyrme forces. It summarizes the correlation effects from low lying 2^+ states.

The uppermost panels show the 2_1^+ excitation energies. The heavier systems distinguish nicely the doubly magic nuclei by large $E(2_1^+)$. The experimental energies drop suddenly when going away from the doubly magic stage while the theoretical results show a somewhat softer transition. That qualitative mismatch is cause by two approximations which are not optimal for doubly-magic nuclei: the LN recipe for stabilized pairing and a simple quadrupole constraint rather than full ATDHF. It is to be noted that the same effect was found in the study of [21] which differs in several details of the treatment but does also employ a collective path from CHF. There are slight quantitative discrepancies in the mid-shell regions. These change with the Skyrme force and can be related to the level density at the Fermi surface. Such variations will be discussed later.

The correlation effects (middle and lower panel) show the expected trends, being minimal at doubly magic points and growing large at mid-shell. The question of interest is how large they actually become. The horizontal lines indicate typical values of acceptable uncertainties in a well fitted Skyrme force, 1 MeV for the energy and about 0.02 fm for charge radii or surface thickness. The lighter systems generally have larger correlation effects, often beyond the desired bounds. Some Z=20 and N=20 systems even have slightly positive correlation energies, with ^{40}Ca being the worst case. That unphysical effect is due to the GOA. It requires smooth collective paths [44]. But for these small semi-magic systems, the abrupt pairing phase transition lies well inside the range of the shape fluctuations of the ground state and it is not sufficiently well smoothed by the LN scheme. An $E_{\rm corr} \approx +0.5\,$MeV is anyway within the expected precision of the method. The ^{40}Ca is more dramatic because the low 2^+ state is not really collective. Besides these critical light nuclei, correlation effects are negative for energies and positive for r.m.s. radii, as it should be. The parameters derived from the charge form factor, diffraction radius and surface thickness can go both ways and do so. The results carry two surprises: first, the form parameters (middle panels) generally show smaller correlation effects relative to the goal than the energies, and second, the correlation energies are large within isotopic chains while remaining moderately small in isotonic chains. Both features call for a revision of fitting strategies. A thorough discussion of reliable data sets for the adjustment of Skyrme parameters will follow in a separate publication. Here we continue with discussing variations of Skyrme forces, pairing, and collective approximations to corroborate the above result. To that end, we confine the presentation to the isotopic Z=50 chain and the isotonic N=82 chain. That contains all necessary trends while rendering the figures more transparent.

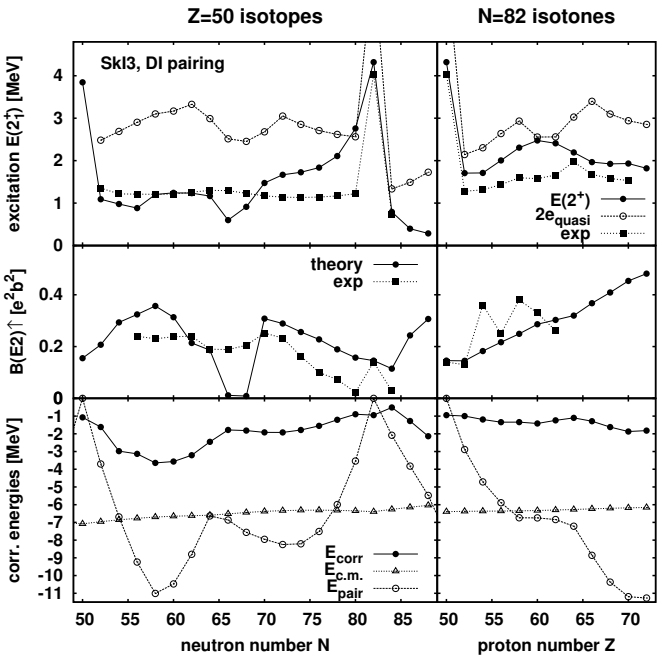

Fig. 2. Collectivity of the low lying 2^+ states for Sn isotopes (left) and $N = 82$ isotones (right) computed with SkI3 and DI pairing. Upper panels: comparison of $E(2_1^+)$ excitation energies, from pure mean field (two quasiparticle energies), full collective calculations, and experiment. Middle panels: $B(E2)\uparrow$ values from collective calculations and experiment. Lower panels: correlation energies.

3.2 Low lying 2^+-excitations

Figure 2 shows more details about the 2_1^+ state and the correlations energies. The upper panel contains the $E(2_1^+)$ excitation energies and adds the two-quasiparticle ($2QP$) energies E_{2QP} for comparison. The difference between the

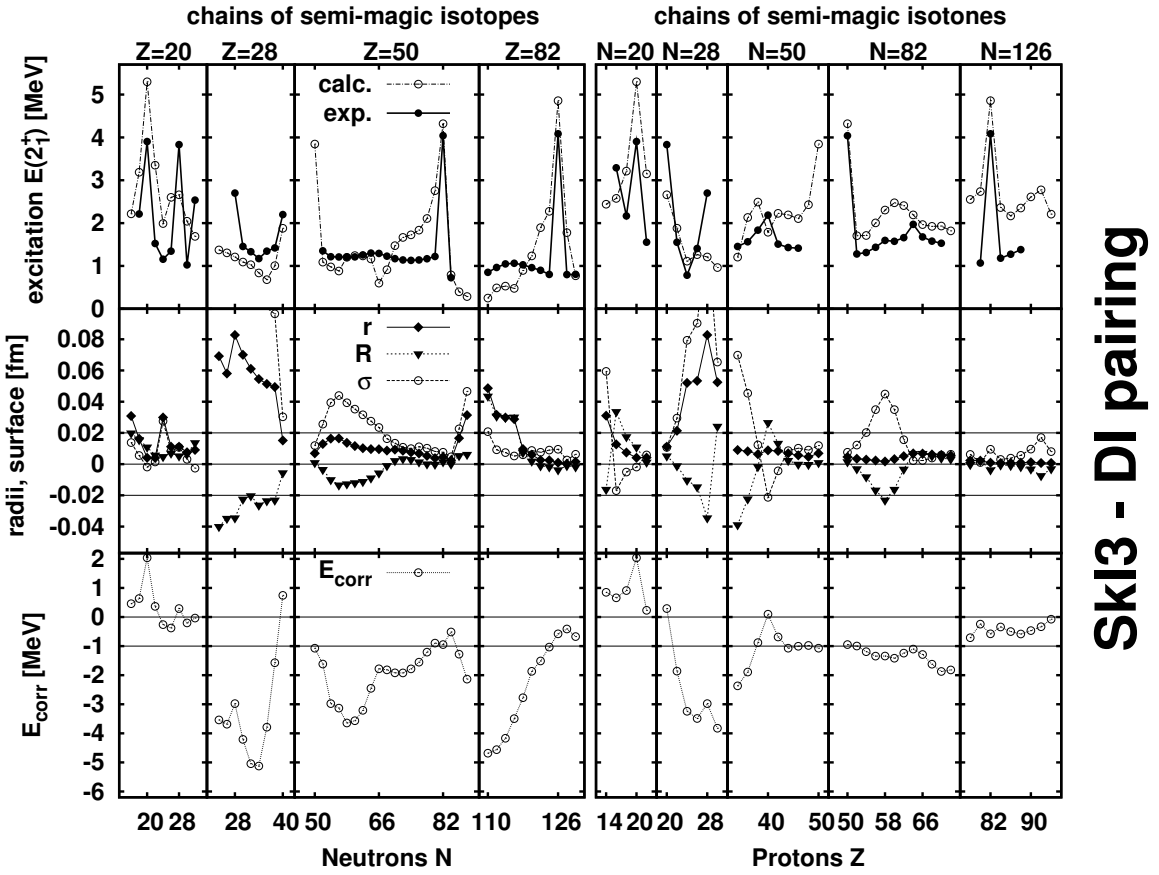

Fig. 1. Correlation effects on semi-magic isotopic (left) and isotonic (right) chains computed with SkI3 and DI pairing. Upper panels: E_2^+ excitation energies, theoretical and experimental as indicated. Middle panels: correlation shifts of charge r.m.s. radii r, diffraction radii R, and surface thicknesses σ. Lower panels: correlation energies.

E_{2QP} and the fully dressed $E(2_1^+)$ characterizes the strength of the residual interaction which is clearly related to the correlation (lowest panels). One also sees the systematic effect that isotones (upper right) have less collective downshift than isotopes (upper left), and thus smaller correlation energy (lowest panels).

The middle panel complements the excitation energies by the corresponding B(E2) values. These agree in the average fairly well with the experimental data (taken from [45,46,47,48,49,50,51,52,53]). However, there are substantial deviations in details: a dramatic drop at N=66 and 68 and a trend to overestimation towards shell closure N=82. The breakdown of the $B(E2)$ in the mid-shell tin isotopes is related to the kink in the $E(2_1^+)$ which, in turn, can be traced back to a kink in the two-quasiparticle energy (upper panel). The reason is the interference with a shape transition which is probably unrealistic, an artefact of that particular force (we see it also for SLy6, but not for SkM* and the other forces discussed here). The differences around the doubly-magic tin isotope result from using the CHF path as an approximation to the optimized ATDHF path. By construction CHF overestimates the collectivity of the ground state and thus also the transition probability to the 2^+-state. The mismatch is similarly seen in the too large excitation energies. The same artefact appears also in studies based on different nucleon-nucleon interactions using a similar collective model based on a CHF path [21] while a recent QRPA study performs much better in that respect [54]. As QRPA can be considered as the small amplitude limit of ATDHF, that result indicates that full ATDHF will cure the mismatch for those isotopes.

The lowest panels show the c.m. correlation energies and pairing energies in addition to the collective correlation energy. The c.m. energy has a very smooth trend because it is related to excitation across shells. The collective correlation energies, on the other hand, are related to intra-shell excitations and thus changing from isotope to isotope. The trend is very similar to the trend of the pairing energy which depends similarly on the available intra-shell phase space.

Figure 3 demonstrates the effect of the collective ground state correlations (GSC) on the trend of the deviation from experimental binding energies. The pure mean-field calculations (open circles) display an unresolved trend for the isotopic chain (left) while having already the correct trend for the isotones (right). The GSC now perfectly compensate that due to strong correction for the mid-shell isotopes (see figure 2). The practically flat trend of the GSC for the isotones leaves their already agreeable pattern intact.

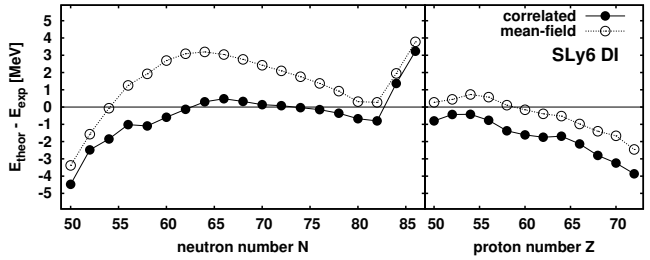

Fig. 3. Difference between theoretically computed and experimental binding energies in Z=50 isotopes (left) and N=82 isotones (right) computed with SLy6 and DI pairing. Compared are pure spherical mean-field calculations (open circles) with correlated ground state energies (filled circles).

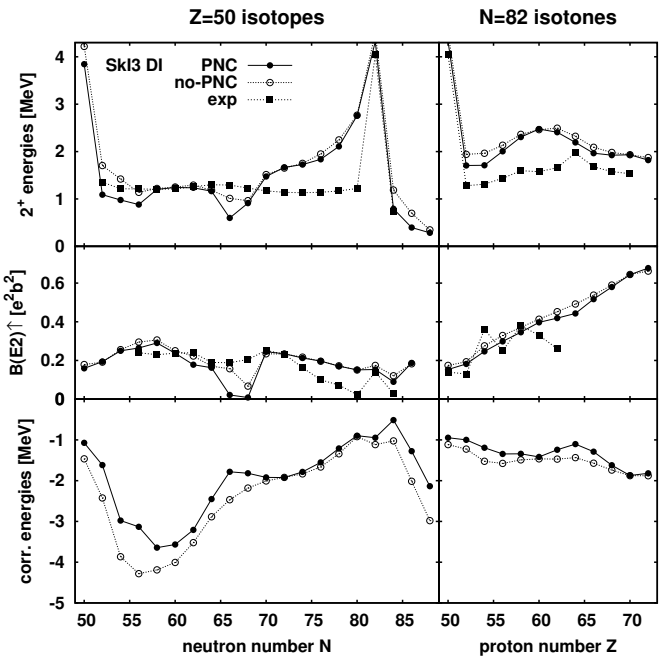

Fig. 4. Effect of the particle-number correction on excitation energies (top) and on correlation energies (bottom) for Sn isotopes (left) and $N = 82$ isotones (right) computed with SkI3 and DI pairing.

3.3 Comparing approximations

Figure 4 shows the effect of particle number correction (PNC) on excitation and correlation energies. The case without PNC means to ignore the term $\propto \delta\epsilon_{\rm F}$ in (3). The effect on $E(2_1^+)$ is small, but the PNC are slightly improving the steepness of the transition from doubly-magic nuclei to semi-magic ones. The effect on correlation energies is still small but noteworthy at a quantitative level. It is particularly interesting that it always reduces $E_{\rm corr}$ while the general trends remain unchanged. The PNC reacts particularly sensitive at N=66 and 68, the region where shape fluctuations lead to the much reduced B(E2) values.

Figure 5 deals with the treatment of the collective mass, comparing results of the (standard) GCM which employs only stationary deformation paths yielding the

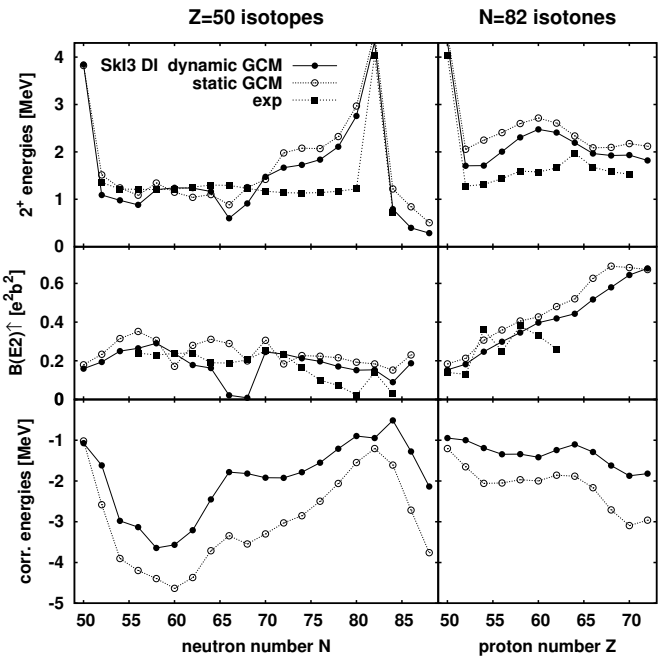

Fig. 5. Effect of the dynamical response ("dynamic GCM") on excitation energies (top) and on correlation energies (bottom) for Sn isotopes (left) and $N = 82$ isotones (right) computed with SkI3 and DI pairing.

redundant mass (7) with the dynamic GCM which explores the dynamical response of the nucleus and so employs the self-consistent cranking mass (6b). The dynamic GCM lowers the $E(2_1^+)$ and improves, in particular, the steepness for the step away from doubly-magic nuclei. The B(E2) values react particularly sensitive at N=66 and 68, precisely the region which is very sensitive for some forces.

For the correlation energies, the trends remain robust qualitatively, but there is a sizeable reduction by about 20-50%. Both trends can be explained by the feature that the dynamical response is a first step towards the fully self-consistent ATDHF path (that is why self-consistent cranking is often called ATDHF cranking). The variation in the larger space reduces the excitation energies and, at the same time, takes a different cut through the collective landscape which eventually reduces correlations [55]. This shows the importance of proper dynamical response and indicates that full ATDHF will improve the performance at and around doubly magic nuclei.

3.4 Variation of the Skyrme- and pairing force

Figure 6 compares results for three widely used Skyrme parameterizations. The global trends of the results are the same: smaller $E_{\rm corr}$ for isotonic chains, overall size of $E_{\rm corr}$, growth of $E_{\rm corr}$ towards mid shell, and too smooth decrease away from doubly-magic nuclei. There are differences in detail. The dip in the $E(2_1^+)$ and B(E2) at ^{116}Sn does not appear for SkM*, and this force also has the correlation maximum at a different position in the isotopic chain.

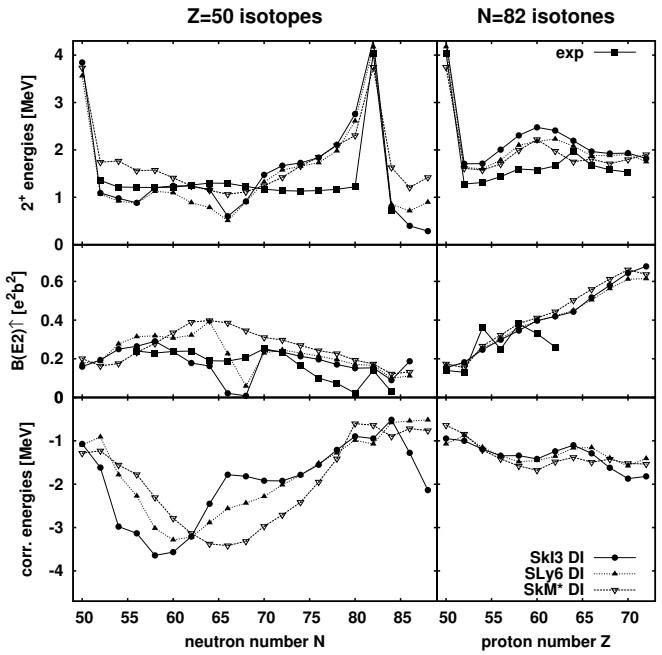

Fig. 6. Correlation energies and 2^+-energies calculated with SkI3, SLy6 and SkM* and DI-pairing.

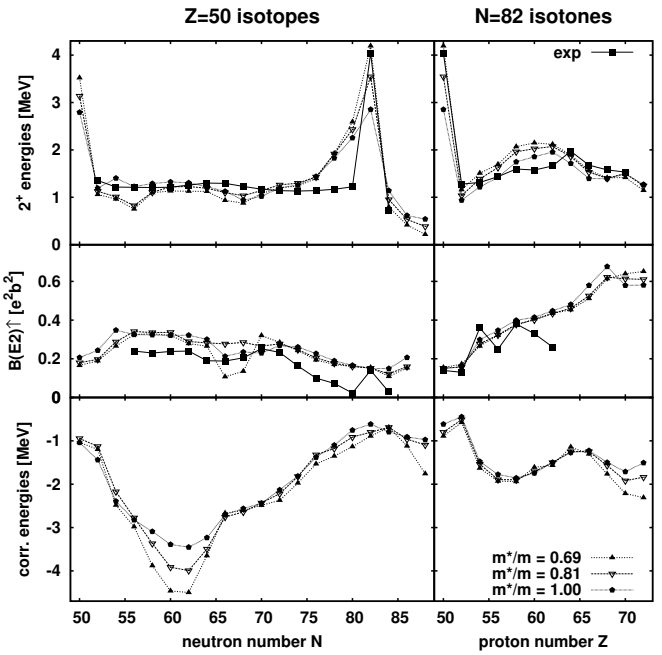

Fig. 7. Influence of the effective nucleon mass m^*/m on excitation energies (top) and on correlation energies (bottom) for Sn isotopes (left) and $N = 82$ isotones (right). Compared are results for three Skyrme forces with systematically varied m^*/m while keeping all other features the same.

It is not possible to judge which of the features of the three forces is most responsible for the slight differences. In order to disentangle the driving agents, we now are considering a series of Skyrme parameterizations produced under the same conditions while varying systematically one selected feature. It originated from a systematic analysis of giant resonances and their dependence on the Skyrme parameters [41]. Figure 7 shows a variation of the effective mass m^*/m. This feature has an impact on the shell structure, mainly the level density. The $E(2_1^+)$ are almost inert. The B(E2) values are also generally inert, but show some sensitivity around the notoriously critical N=66. The same holds for $E_{\rm corr}$ where some effects can be seen in regions around N=60 and N=82 for Sn isotopes and here the correlations increase with decreasing m^*/m as one would expect. The other regions where $E_{\rm corr}$ is less sensitive are dominated by pairing as we will see later. The variation of the symmetry energy shown in figure 8 is very robust and shows even smaller effects.

We also studied other variations of bulk parameters (sum rule enhancement κ, incompressibility, density dependence of $a_{\rm sym}$). Changes in those cases were even smaller.

Figure 9 shows the effect of using different forms for the l·s coupling [41]. Recall that there is some variety in handling the l·s forces for SHF functionals. The standard form is derived from a zero-range two-body l·s interaction [56] which leads to a fixed mix of isoscalar and isovector l·s coupling, the isovector being half as large as the isoscalar one. That is indicated by "stdls" in the figure. The classical limit of the relativistic mean-field model suggests that the isovector spin-orbit should be nearly zero [40], a variant which is indicated by "rmfls" in the plot. Moreover, there is a spin-orbit term $\propto \mathcal{J}^2$ emerging from

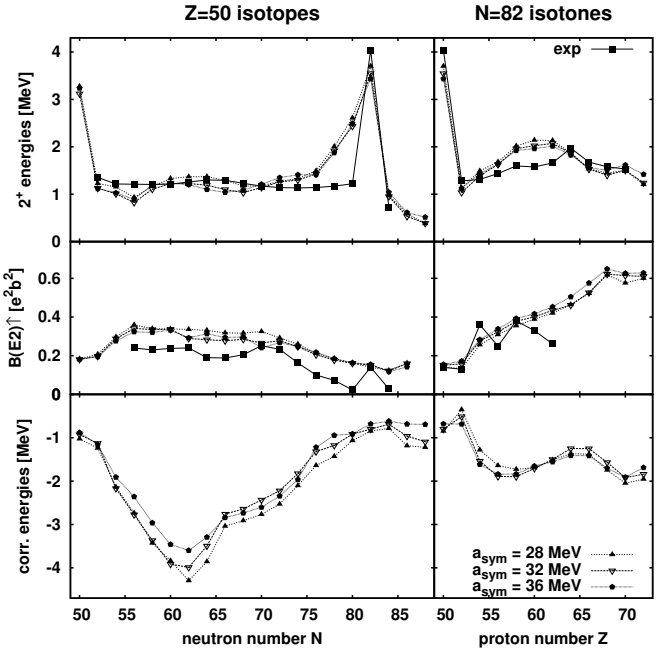

Fig. 8. Influence of the symmetry energy $a_{\rm sym}$ on excitation energies (top) and on correlation energies (bottom) for Sn isotopes (left) and $N = 82$ isotones (right). Compared are results for four Skyrme forces with systematically varied $a_{\rm sym}$ while keeping all other features the same.

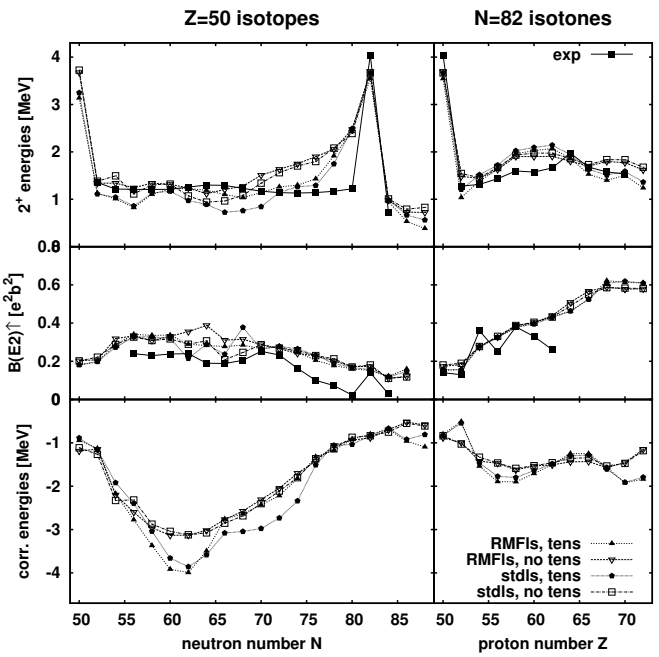

Fig. 9. Influence of the form of the l∗s functional on excitation energies (top) and on correlation energies (bottom) for Sn isotopes (left) and $N = 82$ isotones (right).

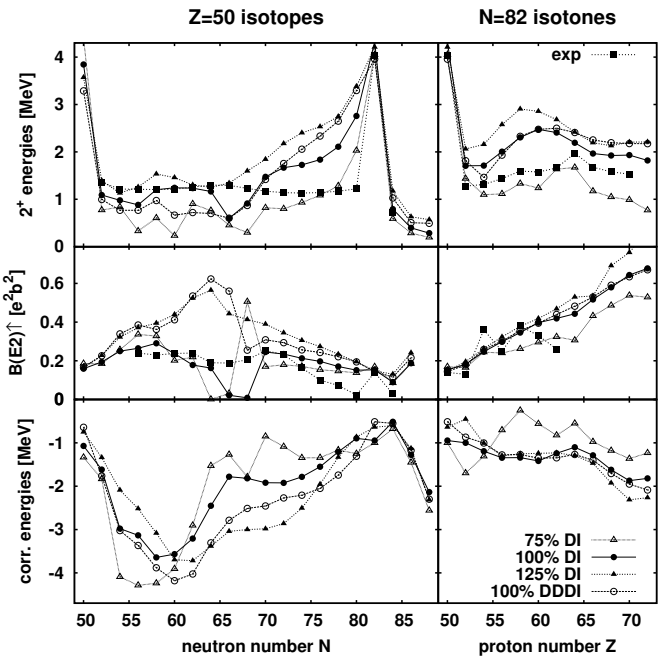

Fig. 10. Influence of the pairing strength and pairing functional on excitation energies (top) and on correlation energies (bottom) for Sn isotopes (left) and $N = 82$ isotones (right). Compared are results for DI pairing with systematically varied strength and DDDI pairing, all for SkI3.

the kinetic zero-range interaction. It is called tensor l·s term. Many parameterizations omit that term. Inclusion is indicated in the figure by "tens" and omission by "no tens". $a_{\rm sym}$ The impact of the different l·s models is well visible: Inclusion of tensor l·s yields somewhat larger correlation energies and lower $E(2^+)$ at places, particularly in combination with the standard l·s model. The B(E2), on the other hand, are robust towards shell closures and show some sensitivity mid shell. It is obvious that the l·s force has a large effect on shell structure. We observe that changing the l·s model can even change the ordering of levels near the Fermi energy. This, in turn, modifies quasi-particle energies and thus $E(2^+)$ as well as $E_{\rm corr}$.

Figure 10 demonstrates the effect of pairing. It shows a variation of the strengths V_{0q} of the pairing functional (1) for the case of DI-pairing relative to the original DI and DDDI pairing functional. The effects are considerable for all three observables shown. Again, the $E(2_1^+)$ are very sensitive due to a close breakdown of pairing for the lower strength. It is noteworthy that DDDI even produces different trends than DI for $E(2_1^+)$. The correlation energies are more robust, yet showing here the largest variations of all cases studied here. The results for the $E(2_1^+)$ in comparison to experiment show that the reduced pairing strength is clearly ruled out. What remains proves again that the trends of correlation energies and their approximate magnitudes are a very robust quantity, a generic feature of all reasonable SHF functionals.

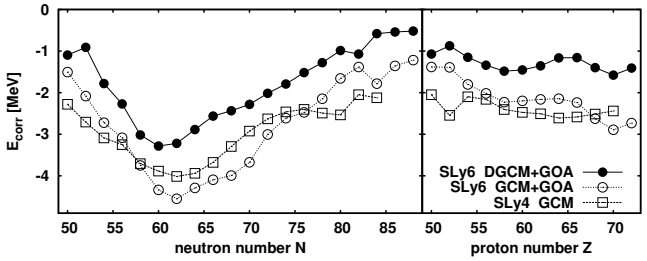

Fig. 11. Comparison of different approximations to the quadrupole correlated state. The DGCM-GOA and GCM-GOA calculations made use of the topological interpolation to recover the full quadrupole configuration space (5D) during the solution of the GCM-GOA Hamiltonian. The GCM calculations are performed directly by coherent superposition of the microscopic states along the static axial path (3D) avoiding the intermediate step of the GOA approximation and the collective Schrödinger equation.

3.5 Comparison with a large-scale GCM analysis

Figure 11 tries a comparison with the GCM calculations of [19,20]. It has to be taken with care because there are several differences at once: The method of [19,20] handles pairing in a slightly different phase space (cutting symmetrically above and below the Fermi energy), it deals with full particle number projection (where we restore particle number in the average), it uses full angular momentum projection (while we do that in GOA), it uses only the stationary path, it performs the collective superposition only within the space of axially symmetric shapes (where

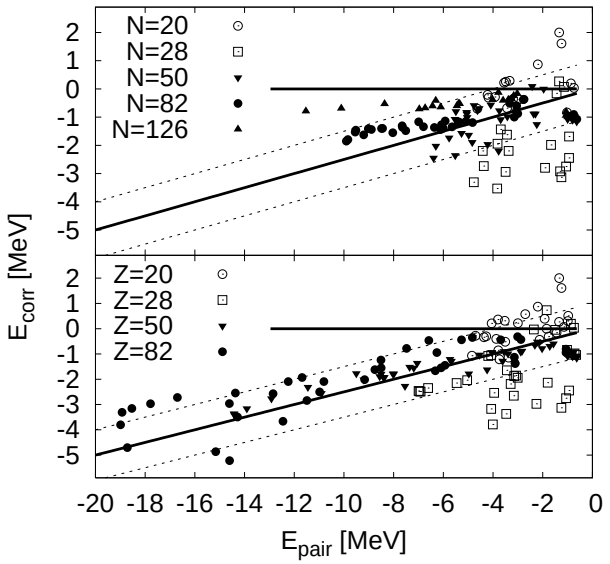

Fig. 12. Correlation diagram between $E_{\rm corr}$ and the pairing energy $E_{\rm pair}$ of the static mean-field ground-state for isotonic chains (upper panel) and isotopic chains (lower panel). The correlation and pairing energies were calculated using the Skyrme parameterizations SkI3, SLy6 and SkM* and DI-pairing. The average linear trend $E_{\rm corr} = 0.25 E_{\rm pair}$ is indicated as the solid line through the scatter while typical deviations of $\pm$1MeV are indicated by the dashed lines.

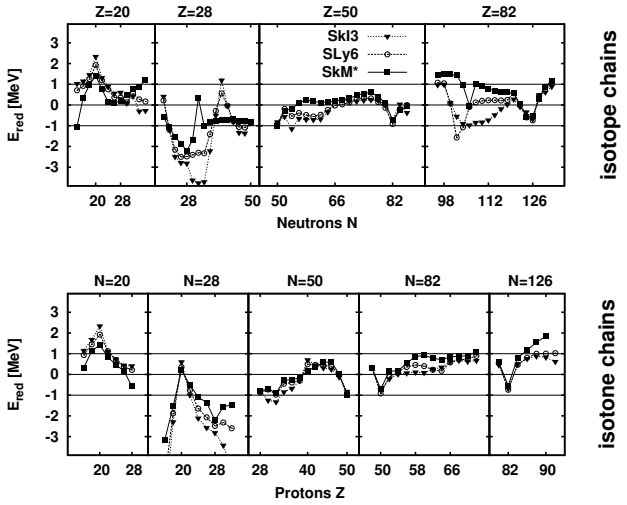

Fig. 13. The reduced correlation $E_{\rm red} = E_{\rm corr} - 0.25 E_{\rm pair}$ drawn versus the proton number Z for the semi-magic isotone chains (upper panel) or neutron number N for the semi-magic isotones (lower panel). As in figure 12 the data were obtained with the three Skyrme parameterizations SkI3, SLy6 and SkM* and DI pairing.

we interpolate to fully triaxial collective dynamics), and it circumvents the collective Schrödinger equation by determining the superposition weights directly through the Hill-Wheeler equation with the given overlap kernels. Finally, we deal with two slightly different forces, SLy4 and SLy6. But these forces belong to the same family and behave very similar such that this should not spoil the comparison. In spite of all differences, the results in figure 11 are quite instructive. First of all, there is an overall agreement in trends and magnitude. Looking more closely, one sees even a close agreement between the full, but static, GCM treatment of [19,20] and our approach at the same level, namely the one using the mere GCM mass (denoted "GCM" in the plot). The main difference seems to come from the self-consistent mass in DGCM. That statement, however, has to be taken with care because the multitude of differences in treatment leaves many options open. It would require a very detailed study to disentangle the various ingredients. This is beyond the scope of the present paper.

3.6 A rough estimate of the average correlation energy

The question arises whether one can establish a relation between the correlation energy and other quantities which are simpler to compute. Pairing properties are the most promising candidates for that purpose because pairing is switched on and off with similar trends as collective correlations. We have figured out that the closest connection exists with the pairing energy (1) of the mean-field ground state. Figure 12 collects results from a variety of forces in a diagram $E_{\rm corr}$ versus $E_{\rm pair}$. The upper panel shows isotopic chains (i.e. neutron pairing) and the lower isotonic ones (i.e. proton pairing) as indicated. The nuclei with large pairing and correlation energies indicate a clear linear trend which we have determined as $E_{\rm corr} = 0.25\, E_{\rm pair}$ by least squares fitting. Small nuclei (open symbols) show a larger scatter, but have smaller correlation energies throughout. The Ni isotopes with Z=28 and the isotones with N=28 are particularly off the line. The fit line is accompanied by two parallel lines indicating the band $\pm$1 MeV. It is gratifying to see that most nuclei with $N, Z \geq 50$ stay fairly well within that band. That nourishes the hope that one may develop a simple formula for previewing correlation effects. It ought to be mentioned, however, that the trend is not so strictly linear for DDDI pairing. This, as well as the strong deviations for the N=126 isotones here, have yet to be understood.

Taking the simple trend from figure 12, we define a reduced correlation energy as $E_{\rm red} = E_{\rm corr} - 0.25\, E_{\rm pair}$. Figure 13 shows the trends of $E_{\rm red}$ over all isotopic and isotonic chains. That shows even better the nice performance for the heavier nuclei and some yet unresolved trends. The latter call yet for refinement of the estimate and, at the same time, may serve to give a clue for the improvement.

4 Conclusions and outlook

Based on nuclear mean-field calculations using the Skyrme energy-density functional, we have studied ground state correlations as produced by the soft modes associated with low-lying quadrupole states. The collective dynamics was

described by a coherent superposition of deformed mean-field states which were produced by quadrupole constrained Skyrme-Hartree-Fock calculations. The information on collective transport (masses, inertia) was evaluated by a self-consistent calculation of the dynamical response to changing deformation. The thus correlated state was handled with the generator-coordinate method (GCM) in the Gaussian overlap approximation (GOA) yielding effectively a collective Hamiltonian in quadrupole coordinates and similar mapping of other observables. The study concentrated on semi-magic nuclei with more or less shape fluctuations about the spherical shape. The microscopic mean-field calculations employed axially symmetric deformations while the collective dynamics was considered with all five quadrupole degrees of freedom by properly interpolating the collective properties (potential, masses and quantum corrections) into the triaxial plane. The procedure was employed for a systematic exploration of ground state correlations on nuclear bulk properties (energy, radii, surface thickness) scanning its dependence on the underlying energy functional and on detailed corrections as, e.g., restoration of particle number or dynamical response. We have also investigated the energies and B(E2) values of the low-lying 2^+ excitation.

On the side of the model development, we find that the proper treatment of dynamical response has moderate effect on $E(2_1^+)$ excitation energies (about 10–20%) but a huge one on correlations (factor two on $E_{\rm corr}$). The restoration of the correct particle number makes less effects, a few percent on $E(2_1^+)$ and about 10% on $E_{\rm corr}$. We also find that the low lying quadrupole state is a truly large-amplitude mode. Even in doubly magic ^{208}Pb, a small amplitude limit turns out to be unreliable (15% effect on $E(2_1^+)$). Some small nuclei cause problems in that they have a positive correlation energy. The GOA becomes insufficient there due to a small number of nucleons involved in the motion (lack of collectivity) and due to a strong impact of the pairing phase transition. For system sizes, the trends of $E(2_1^+)$ do not reproduce the experimentally found steep decrease when going away from doubly-magic nuclei. This defect was also found in earlier calculations using GCM. That is a problem of the simple quadrupole constraint used for generating the collective path. More elaborate schemes as, e.g., adiabatic time-dependent Hartree-Fock are required to describe correctly the transition from collectivity in mid-shell nuclei to predominantly two-quasiparticle excitations in doubly-magic systems.

The large scale variation of energy functionals has shown that the correlation effects are very robust. Their trends and magnitudes come out quite similarly for all Skyrme forces in this survey. Even the more sensitive 2^+ excitation shows very similar patterns throughout. Differences are seen, of course, in detail. Variation of bulk properties as symmetry energy or effective mass has little effect. Somewhat more sensitivity is seen for variations of the spin-orbit model, in particular tensor spin-orbit can produce up to 20% on $E_{\rm corr}$ and 40% on $E(2_1^+)$. The strongest effect comes from variation of the pairing strength. Particularly the $E(2_1^+)$ are very sensitive which is no surprise because of known strong interplay between shape transitions and pairing. However, the basic result of the robustness of $E_{\rm corr}$ remains valid even here. We have also found a close relation between $E_{\rm corr}$ and the pairing energy of the mean-field ground state which show in the average a linear dependence on each other.

The results provide clear indications for the next steps. On the formal side, one needs to go for the self-consistent constraints according to ATDHF replacing the simple-minded quadrupole constraint and one should search for a better smoothing of the pairing phase transition, if possible. For further applications, one can take advantage of the robust information on correlation effects and use these as guide for searching least correlated ground state observables as input for better adjustments of Skyrme energy functionals. It is also worth while to improve the estimate of correlations energies in terms of simple to compute quantities. Work in all these directions is in progress.

Acknowledgments

That work was supported by the BMBF contract number 06 ER 124D. We thank M. Bender, T. Bürvenich and J. Erler for helpful discussions. We thank G. Hager and the Regional Computing Center Erlangen for help in performing the large computing tasks.

A Interpolating the Collective Hamiltonian

A.1 Intrinsic system

The Cartesian representation of the quadrupole coordinates (α_μ) is advantageous for formulating the GCM-GOA Hamiltonian (4). For the solution of the collective Schrödinger equation a formulation in terms of the intrinsic coordinates $(\beta, \gamma, \boldsymbol{\vartheta})$ is more convenient [23,57,24]:

$$\alpha^\mu = \beta \left\{ \cos(\gamma) D^{2*}_{\mu,0}(\boldsymbol{\vartheta}) + \sin(\gamma) \frac{D^{2*}_{\mu,+2}(\boldsymbol{\vartheta}) + D^{2*}_{\mu,-2}(\boldsymbol{\vartheta})}{\sqrt{2}} \right\} . \tag{8}$$

The shape of the nucleus is parameterized in one of the principal axes systems of the nucleus by the total deformation β and triaxiality γ while the orientation of this principal axis system is given by the three Euler angles $\boldsymbol{\vartheta}$. The representation of the collective Hamiltonian in these coordinates is advantageous due to the decoupling of rotation and vibration modes. In detail the collective Hamiltonian reads

$$\hat{H} = \boldsymbol{\nabla}^\dagger \mathbf{B}(\beta,\gamma) \boldsymbol{\nabla} + V(\beta,\gamma) , \tag{9a}$$

with collective potential V, mass tensor

$$\mathbf{B} = \begin{pmatrix} B_{\beta\beta} & B_{\beta\gamma} & 0 & 0 & 0 \\ B_{\beta\gamma} & B_{\gamma\gamma} & 0 & 0 & 0 \\ 0 & 0 & B_x & 0 & 0 \\ 0 & 0 & 0 & B_y & 0 \\ 0 & 0 & 0 & 0 & B_z \end{pmatrix} , \tag{9b}$$

and the gradient

$$\boldsymbol{\nabla} = \left(\partial_\beta, \tfrac{1}{\beta}\partial_\gamma, \tfrac{\mathrm{i}\hat{L}'_x}{2\beta\sin(\gamma-\frac{2\pi}{3})}, \tfrac{\mathrm{i}\hat{L}'_y}{2\beta\sin(\gamma-\frac{4\pi}{3})}, \tfrac{\mathrm{i}\hat{L}'_z}{2\beta\sin(\gamma)}\right)^t . \tag{9c}$$

It is important to note that the components of the collective mass tensor as well as the potential depend on the deformation coordinates (β,γ) but not on the orientation of the intrinsic system $(\boldsymbol{\vartheta})$. The actual orientation of the system is incorporated by the angular momentum operators of the intrinsic system $\hat{L}'_k = \hat{L}'_k(\boldsymbol{\vartheta})$ $(k \in (x,y,z) \equiv (1,2,3))$. The choice of the intrinsic system is not unique, which results in additional symmetry conditions:

$$(\beta,\gamma) = X(\beta,\gamma - k\tfrac{2\pi}{3}) , \tag{10a}$$

$$B_k(\beta,\gamma) = B_z(\beta,\gamma - k\tfrac{2\pi}{3}) \tag{10b}$$

with $X \in \{V, B_{\beta\beta}, B_{\gamma\gamma}, B_{\beta\gamma}\}$ which have to be fulfilled necessarily by the collective parameter functions [57].

A.2 Expansion of Collective Potential and Masses

Following similar lines to the rotationally invariant expansion of the generalized Bohr-Hamiltonian in [57] a symmetry conforming, polynomial expansion of the collective potential and mass tensor can be derived by appropriate coupling of the spherical tensors of coordinates $\boldsymbol{\alpha}$ and conjugate momenta $\boldsymbol{\pi}$.

To account for the fluctuations of the collective potential with deformation β while assuming a smooth interpolation in the triaxial degree of freedom, the polynomial expansion of the collective potential V is approximated up to lowest order in γ while maintaining symmetry requirements and the most general β-dependency similar to [33]:

$$V(\beta,\gamma) = V_1(\beta) + \beta^3\cos(3\gamma)V_1(\beta) . \tag{11}$$

By means of similar arguments the γ-smooth parameterization of the collective mass tensor is given in (12). To end up with a polynomial expansion the functions $V_i(\beta), B_i(\beta)$ have to be analytic and even functions.

A.3 Interpolation Formulas

The parameterization of the collective potential (11) and mass (12) are adjusted to the values obtained by CHF and cranking along the axially symmetric cuts ($\alpha^0 = \alpha_{20}, \alpha^{\pm 2} = \alpha^{\pm 1} = 0$). Besides the Born-Oppenheimer surface $V(\alpha_{20})$ the three dimensional axial GCM-GOA Hamiltonian is defined from the β-vibrational mass $B_{\beta\beta}(\alpha_{20})$ corresponding to motion along the axial symmetric path and the degenerate rotational mass $B_{x/y}(\alpha_{20})$ related to rotations around the non-symmetry axes. Generalizing the collective Hamiltonian to the five dimensional configuration space yields the simple interpolation rules between the expansion coefficients in (12) and the collective parameter functions obtained from the axial calculations:

$$V_0(\beta) = \frac{V^{(\mathrm{p})} + V^{(\mathrm{o})}}{2} , \tag{13a}$$

$$V_1(\beta) = \frac{V^{(\mathrm{p})} - V^{(\mathrm{o})}}{2\beta^3} , \tag{13b}$$

$$B_1(\beta) = \frac{1}{10}\left[2B^{(\mathrm{p})}_{\beta\beta} + 2B^{(\mathrm{o})}_{\beta\beta} + 3B^{(\mathrm{p})}_{x/y} + 3B^{(\mathrm{o})}_{x/y}\right], \tag{13c}$$

$$B_2(\beta) = \frac{1}{7\beta}\left[2B^{(\mathrm{p})}_{\beta\beta} - 2B^{(\mathrm{o})}_{\beta\beta} + 3B^{(\mathrm{p})}_{x/y} - 3B^{(\mathrm{o})}_{x/y}\right], \tag{13d}$$

$$B_3(\beta) = \frac{3}{10\beta^2}\left[B^{(\mathrm{p})}_{\beta\beta} + B^{(\mathrm{o})}_{\beta\beta} - B^{(\mathrm{p})}_{x/y} - B^{(\mathrm{o})}_{x/y}\right], \tag{13e}$$

$$B_4(\beta) = \frac{3}{14\beta^3}\left[B^{(\mathrm{p})}_{\beta\beta} - B^{(\mathrm{o})}_{\beta\beta} - 2B^{(\mathrm{p})}_{x/y} + 2B^{(\mathrm{o})}_{x/y}\right], \tag{13f}$$

where $X^{(\mathrm{p})} = X(\alpha_{20} = \beta)$ and $X^{(\mathrm{o})} = X(\alpha_{20} = -\beta)$. By inserting the expansion functions B_i and V_i into (12) the collective mass tensor and potential are found.

A.4 Zero-Point Energies

The zero-point energies (ZPE) are composed from the interpolated potential $V(\beta,\gamma)$, the mass tensor $\mathbf{B}(\beta,\gamma)$ and the GOA width tensor $\boldsymbol{\lambda}(\beta,\gamma)$. Thereby the width tensor is interpolated in the same manner as the collective mass tensor. In the-five dimensional case the zero-point energy correction also includes terms from spurious ZPE in the additional degrees of freedom, namely the γ-vibration and z-rotation mode as well as contributions from the β-γ-coupling. The contributions from the kinetic ZPE are constructed straight forward from the parameter functions by

$$\begin{aligned} E^{\mathrm{ZPE}}_{\mathrm{kin}} &= \frac{1}{2}\lambda_{\mu\nu}B^{\mu\nu} \\ &= \frac{1}{2}\left[\lambda_{\beta\beta}B_{\beta\beta} + \lambda_{\gamma\gamma}B_{\gamma\gamma} + 2\lambda_{\beta\gamma}B_{\beta\gamma} + \sum_{k=x,y,z}\lambda_k B_k\right] . \end{aligned} \tag{14}$$

A compact notation of the potential ZPE requires to define the curvature tensor of the collective potential $C_{\mu\nu} = \frac{1}{2}\nabla_\mu\nabla_\nu V$ with intrinsic components

$$\begin{aligned} C_{\beta\beta} &= \frac{1}{2}\partial^2_\beta V(\beta,\gamma) , \\ C_{\gamma\gamma} &= \frac{1}{2}\left[\frac{1}{\beta}\partial_\beta + \frac{1}{\beta^2}\partial^2_\gamma\right] V(\beta,\gamma) , \\ C_{\beta\gamma} &= \frac{1}{2}\left[\frac{1}{\beta}\partial_\beta\partial_\gamma - \frac{1}{\beta^2}\partial_\gamma\right] V(\beta,\gamma) , \\ C_k &= \frac{1}{2}\left[\frac{1}{\beta}\partial_\beta + \frac{\cot(\gamma - k\frac{2\pi}{3})}{\beta^2}\partial_\gamma\right] V(\beta,\gamma) . \end{aligned} \tag{15}$$

In terms of the components of the curvature tensor $\mathbf{C}$ the potential ZPE is evaluated in analogy to the kinetic ZPE

$$
\begin{aligned}
B_{\beta\beta}(\beta,\gamma) &= B_1(\beta) + \beta\cos(3\gamma)B_2(\beta) + \beta^2 B_3(\beta) + \beta^3\cos(3\gamma)B_4(\beta)\ ,\\
B_{\beta\gamma}(\beta,\gamma) &= \qquad -\beta\sin(3\gamma)B_2(\beta) \qquad\quad - \frac{5\beta^3}{12}\sin(3\gamma)B_4(\beta)\ ,\\
B_{\gamma\gamma}(\beta,\gamma) &= B_1(\beta) - \beta\cos(3\gamma)B_2(\beta) + \frac{\beta^2}{6}B_3(\beta) + \frac{\beta^3}{6}\cos(3\gamma)B_4(\beta)\ ,\\
B_z(\beta,\gamma) &= B_1(\beta) - \beta\cos(\gamma)B_2(\beta) - \frac{\beta^2}{18}\left(7-10\cos(2\gamma)\right)B_3(\beta) - \frac{\beta^3}{18}\left(7\cos(3\gamma)-10\cos(\gamma)\right)B_4(\beta)\ . \qquad (12)
\end{aligned}
$$

and reads

$$
\begin{aligned}
E_{\rm pot}^{\rm ZPE} &= \frac{1}{2}(\lambda^{-1})^{\mu\nu}C_{\mu\nu} \qquad (16)\\
&= \frac{1}{2}\left[\lambda_{\beta\beta}^{-1}C_{\beta\beta} + \lambda_{\gamma\gamma}^{-1}C_{\gamma\gamma} + 2\lambda_{\beta\gamma}^{-1}C_{\beta\gamma} + \sum_{k=x,y,z}\lambda_k^{-1}C_k\right]\ .
\end{aligned}
$$

The topological interpolation scheme (11, 12) enforces the asymptotic behavior for the ZPEs when approaching the spherical limit: As expected from the harmonic approximation the contributions from the two vibrational modes and the three rotational modes degenerate yielding five equivalent contributions for $\beta = 0$. This feature of our model enables an improved description of ground state properties of magic and especially doubly-magic nuclei.

References

1. W.H. Dickhoff, H. Müther, Rep. Prog. Phys. **55**, 1947 (1992)
2. P.G. Reinhard, C. Toepffer, Int. J. Mod. Phys. **E3**, 435 (1994)
3. V.R. Pandharipande, I. Sick, P.K.A. deWitt Huberts, Rev. Mod. Phys. **69**, 981 (1997)
4. P. Navratil, J.P. Vary, B.R. Barrett, Phys. Rev. C **62**, 054311 (2000)
5. C. Fuchs, Prog. Part. Nuc. Phys. **56**, 1 (2006)
6. J.W. Negele, D. Vautherin, Phys. Rev. **C5**, 1472 (1972)
7. M. Bender, P.H. Heenen, P.G. Reinhard, Rev. Mod. Phys. **75**, 121 (2003)
8. R.M. Dreizler, E.K.U. Gross, *Density Functional Theory* (Springer, Berlin, Heidelberg, New York, 1990)
9. P.G. Reinhard, J. Friedrich, N. Voegler, Z. Phys. **A316**, 207 (1984)
10. M. Koskinen, P.O. Lipas, M. Manninen, Nucl. Phys. A **591**, 421 (1995)
11. T.R. Werner, J. Dobaczewski, M.W. Guidry, W. Nazarewicz, J.A. Sheikh, Nucl. Phys. **A578**, 1 (1994)
12. S. Raman, C.H. Malarkey, W.T. Milner, C.W. Nestor, Jr., P.H. Stelson, At. Data Nucl. Data Table **36**, 1 (1987)
13. P.G. Reinhard, D. Drechsel, Z. Phys. **A290**, 85 (1979)
14. F. Barranco, R.A. Broglia, Phys. Lett. **B151**, 90 (1985)
15. M. Girod, P.G. Reinhard, Nucl. Phys. **A384**, 179 (1982)
16. M. Girod, P.G. Reinhard, Phys. Lett. **117B**, 1 (1982)
17. P. Bonche, J. Dobaczewski, H. Flocard, P.H. Heenen, J. Meyer, Nucl. Phys. **A510**, 466 (1990)
18. P. Bonche, J. Dobaczewski, H. Flocard, P.H. Heenen, Nucl. Phys. **A530**, 149 (1991)
19. M. Bender, G.F. Bertsch, P.H. Heenen, Phys. Rev. Lett. **94**, 102503 (2005)
20. M. Bender, G.F. Bertsch, P.H. Heenen, Phys. Rev. C **73**, 034322 (2006)
21. B. Sabbey, M. Bender, G.F. Bertsch, P.H. Heenen, Phys. Rev. C **75**, 044305 (2007)
22. B. G. F, M. Girod, S. Hilaire, J.P. Delaroche, H. Goutte, S. Péru, Phys. Rev. Lett. **99**, 032502 (2007)
23. A. Bohr, Mat. Fys. Medd. K. Dan. Vidensk. Selsk **26**, No. 14 (1952)
24. G. Gneuss, W. Greiner, Nucl. Phys. A **171**, 449 (1971)
25. F. Iachello, A. Arima, *The Interacting Boson Model* (Cambridge University Press, Cambridge, England, 1987)
26. D.L. Hill, J.A. Wheeler, Phys. Rev. **89**, 1102 (1953)
27. J.J. Griffin, J.A. Wheeler, Phys. Rev. **108**, 311 (1957)
28. P.G. Reinhard, K. Goeke, Rep. Prog. Phys. **50**, 1 (1987)
29. A. Valor, P.H. Heenen, P. Bonche, NP **A671**, 145 (2000)
30. R.R. Rodriguez-Guzmán, J.L. Egido, L.M. Robledo, Phys. Rev. C **65**, 024304 (2002)
31. J. Libert, M. Girod, J.P. Delaroche, Phys. Rev. C **60**, 054301 (1999)
32. L. Prochniak, P. Quentin, D. Samsoen, J. Libert, Nucl. Phys. A **730**, 59 (2004)
33. P. Fleischer, P. Klüpfel, P.G. Reinhard, J.A. Maruhn, Phys. Rev. C **70**, 054321 (2004)
34. M. Bender, K. Rutz, P.G. Reinhard, J.A. Maruhn, Eur. Phys. J. **A8**, 59 (2000)
35. K. Rutz, J.A. Maruhn, P.G. Reinhard, W. Greiner, Nucl. Phys. **A590**, 680 (1995)
36. R.Y. Cusson, P.G. Reinhard, M.R. Strayer, J.A. Maruhn, W. Greiner, Z. Phys. A **320**, 475 (1985)
37. K. Goeke, P.G. Reinhard, Ann. Phys. (NY) **112**, 328 (1978)
38. J. Bartel, P. Quentin, M. Brack, C. Guet, H.B. Håkansson, Nucl. Phys. **A386**, 79 (1982)
39. E. Chabanat, P. Bonche, P. Haensel, J. Meyer, R. Schaeffer, Nucl. Phys. **A627**, 710 (1997)
40. P.G. Reinhard, H. Flocard, Nucl. Phys. **A584**, 467 (1995)
41. P.G. Reinhard (Nucl. Phys., 1999), Vol. A649, pp. 305c–314c
42. P.G. Reinhard, Ann. Phys. (Leipzig) **1**, 632 (1992)
43. National Nuclear Data Center. Information extracted from the NuDat 2 database (accessed 17/11/2007), `http://www.nndc.bnl.gov/nudat2.`
44. P.G. Reinhard, Nucl. Phys. **A261**, 291 (1976)
45. T. Belgya, D. Seckel, E.L. Johnson, E.M. Baum, D.P. DiPrete, D. Wang, S.W. Yates, Phys. Rev. C **47**(1), 392 (1993)

46. J. Bryssinck, L. Govor, V.Y. Ponomarev, F. Bauwens, O. Beck, D. Belic, P. von Brentano, D. De Frenne, T. Eckert, C. Fransen et al., Phys. Rev. C **61**(2), 024309 (2000)
47. C. Vaman, C. Andreoiu, D. Bazin, A. Becerril, B.A. Brown, C.M. Campbell, A. Chester, J.M. Cook, D.C. Dinca, A. Gade et al., Phys. Rev. Lett. **99**, 162501 (2007)
48. C.J. Barton, M.A. Caprio, D. Shapira, N.V. Zamfir, D.S. Brenner, R.L. Gill, T.A. Lewis, J.R. Cooper, R.F. Casten, C.W. Beausang et al., Phys. Lett. **551B**, 269 (2003)
49. J. Gableske, A. Dewald, H. Tiesler, M. Wilhelm, T. Klemme, O. Vogel, I. Schneider, R. Peusquens, S. Kasemann, K.O. Zell et al., Nucl. Phys. **A691**, 551 (2001)
50. D. Radford, C. Baktash, J. Beene, B. Fuentes, A. Galindo-Uribarri, J.G. del Campo, C. Gross, M. Halbert, Y. Larochelle, T. Lewis et al., Nucl. Phys. **A746**, 83 (2004)
51. D. Radford, C. Baktash, C. Barton, J. Batchelder, J. Beene, C. Bingham, M. Caprio, M. Danchev, B. Fuentes, A. Galindo-Uribarri et al., Nucl. Phys. **A752**, 264 (2005)
52. K.H. Speidel, H. Busch, S. Kremeyer, U. Knopp, J. Cub, M. Bussas, W.Karle, K. Freitag, U. Grabowy, J. Gerber, Nucl. Phys. **A552**, 140 (1993)
53. D. Bazzacco, F. Brandolini, K. Löwenich, P. Pavan, C. Rossi-Alvarez, E. Maglione, M. de Poli, , A.M.I. Haque, Nucl. Phys. **A533**, 541 (1991)
54. J. Terasaki, J. Engel, Phys. Rev. C **74**, 044301 (2006)
55. P.G. Reinhard, K. Goeke, Phys. Rev. C **20**, 1546 (1979)
56. D. Vautherin, D.M. Brink, Phys. Lett. **32B**, 149 (1970)
57. K. Kumar, M. Baranger, Nucl. Phys. A **92**, 608 (1967)